Molecular-Docking-Guided Design, Synthesis, and Biologic Evaluation of Radioiodinated Quinazolinone Prodrugs

Kai Chen, Ayman F. Al Aowad, S. James Adelstein, and Amin I. Kassis*

Department of Radiology, Harvard Medical School, Boston, Massachusetts 02115

Enzyme-mediated cancer imaging and therapy (EMCIT) is a novel approach in which radioactive water-soluble molecules are precipitated in vivo following their hydrolysis by extracellular enzymes overexpressed by cancer cells. AutoDock 3.0 was used to model the interaction−binding between a series of iodinated quinazolinone derivatives and human placental alkaline phosphatase (PLAP, crystal structure in the Protein Data Bank) and to assess the effects of structural modification of the derivatives. Ammonium 2-(2′,4′-diphosphoryloxyphenyl)-6-iodo-4-(3H)-quinazolinone (IQ$_{2−P,4−P}$), having the most favorable calculated inhibition constant, was synthesized and characterized. Concentration-dependent, PLAP-mediated conversion of IQ$_{2−P,4−P}$ (**4**)/^{125}IQ$_{2−P,4−P}$ (**6**) to water-insoluble 2-(2′,4′-dihydroxyphenyl)-6-[^{127}I/^{125}I]iodo-4-(*3H*)-quinazolinone (^{127}IQ$_{2−OH,4−OH}$ (**2**)/^{125}IQ$_{2−OH,4−OH}$ (**7**)) was observed in solution. Autoradiography indicated that **6** is hydrolyzed by human cancer cells and the resulting **7** precipitates on exterior cell surfaces. Biodistribution studies in mice demonstrated that **6** is minimally retained by normal tissues. The findings support the validity of the EMCIT approach.

Introduction

One of the current strategies for providing substantial increases in the clinical efficacy of antiproliferative agents that preferentially kill dividing cells, both normal and tumor, is the use of relatively nontoxic prodrug forms that can be selectively activated in tumor tissue.[1] Prodrugs are generally defined as agents that are transformed after administration, either by metabolism or spontaneous chemical breakdown, to pharmacologically active species. During the past two decades, several prodrug-based therapy approaches have been reported, among which two have demonstrated credibility, namely, antibody-directed enzyme−prodrug therapy (ADEPT[a]) and gene-directed enzyme−prodrug therapy (GDEPT). In ADEPT, which was originally described by Philpott[2] and later pursued by Bagshawe[3−5] and Senter,[6] a noninternalizing antitumor-antibody−enzyme conjugate is injected into a tumor-bearing animal prior to the administration of a chemotherapeutic agent (prodrug). The enzyme is selected for its ability to convert the relatively noncytotoxic prodrug into a highly cytotoxic drug. Experimental studies[7,8] have established that the injection of prodrugs into tumor-bearing animals preinjected with monoclonal-antibody−enzyme conjugates will lead to tumor regression and delay in tumor growth. The alternative concept of GDEPT[9] employs a variety of vector systems (liposomes, replicating and nonreplicating viruses, anaerobic bacteria) to deliver and express the gene coding for an exogenous enzyme in tumor cells. The most widely studied GDEPT method involves the thymidine kinase enzyme from the Herpes simplex virus (HSV-TK) in conjunction with the antiviral drug ganciclovir.[10] This enzyme selectively changes ganciclovir to its monophosphate.[11] This compound is then converted by cellular enzymes to the triphosphate,[12] which is toxic because it is incorporated into DNA. Although applications of ADEPT and GDEPT in cancer therapy have been reported by many investigators, these two approaches have several intrinsic limitations, including the relatively long biologic half-lives of the agents, increasing nonspecific normal-tissue toxicity, and loss of prodrug selectivity.

An ideal radiolabeled cancer imaging and therapy agent must (i) be taken up rapidly and efficiently by the tumor, (ii) be retained by the tumor, (iii) not be taken up by normal tissue cells, (iv) have a short residence in normal tissues, (v) achieve high tumor-to-normal-tissue uptake ratios, and (vi) be labeled with an emitter whose decay characteristics are suitable for imaging (PET or SPECT) or therapy. We have been developing a novel technology (enzyme-mediated cancer imaging and therapy, EMCIT) that aims to concentrate radioactive molecules within solid tumors.[13−17] The approach involves enzyme-dependent and tumor-specific in vivo precipitation of a radioactive molecule within solid tumors. In one of its embodiments, a water-soluble radioactive prodrug is hydrolyzed to its water-insoluble form by an enzyme that is *specifically overexpressed* on the exterior surface of tumor-cell plasma membranes. Upon enzymatic hydrolysis, the prodrug molecule loses its prosthetic group, and the resulting compound is water-insoluble and precipitates within the extracellular space of the targeted solid tumor (Figure 1). In EMCIT, the substrates may be radiolabeled with a gamma-, positron-, or energetic-particle-emitting radionuclide. Once the prodrug is precipitated and trapped within the tumor, the prolonged residence time of the drug should permit imaging (SPECT/PET) or the delivery of a high radiation dose to the tumor versus a low dose to the rest of the body. The EMCIT approach takes advantage of the above-mentioned ADEPT and GDEPT methods while overcoming their limitations. Since many tumors (e.g., ovarian, breast, prostate, lung, teratocarcinoma) have been shown to express innately various phosphatases,[18,19] we selected alkaline phosphatase (AP) as our preliminary target[14−17] to ascertain the validity of the approach.

Alkaline phosphatases (EC 3.1.3.1), common to almost all organisms, form a large family of dimeric enzymes and function

---

* To whom correspondence should be addressed at Harvard Medical School, Armenise Building, Room 137, 200 Longwood Ave., Boston, MA 02115; Telephone: (617) 432-7777; Fax: (617) 432-2419; E-mail: amin_kassis@hms.harvard.edu.

[a] Abbreviations: EMCIT, enzyme-mediated cancer imaging and therapy; PLAP, placental alkaline phosphatase; ADEPT, antibody-directed enzyme−prodrug therapy; GDEPT, gene-directed enzyme−prodrug therapy; PDB, protein data bank; RMSD, root mean square deviation; ID/g, injected dose per gram.
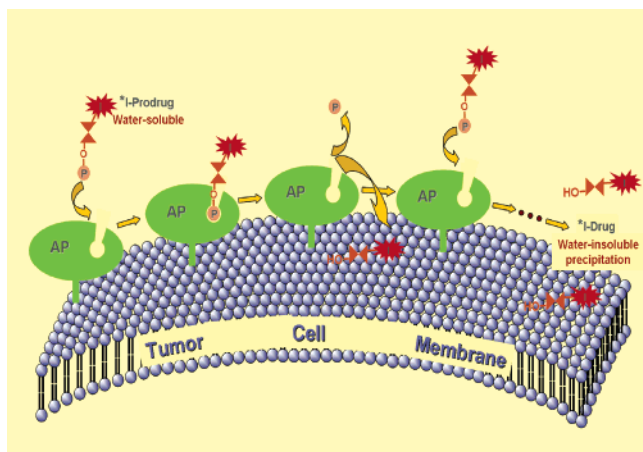
Figure 1. Enzyme-mediated cancer imaging and therapy (EMCIT) approach with alkaline phosphatase (AP) as example; (*I = ^{123}I/^{124}I/^{125}I/^{131}I).

through a phosphoseryl intermediate to produce free inorganic phosphate or to transfer the phosphoryl group to other alcohols.[20,21] All mammalian AP have closely related sequences, conserving three specific elements: the glycosylation sites, the four cysteines involved in the disulfide bridges, and the residues that coordinate metal ions, including zinc and magnesium, in the active-site region. There are at least four AP isozymes in man. Three of these isozymes are tissue-specific, including PLAP (placental), GCAP (germ cell), and IAP (intestinal). Their genes are clustered on the same chromosome, and sequence alignments indicate they are 90%−98% homologous.[22] PLAP has been used extensively in experimental studies,[23−27] including immunohistochemical detection of Regan isoenzyme in cancer cells,[24] determination of placental-like alkaline phosphatase in malignant and benign ovarian tumors,[26] and assessment of placental-like alkaline phosphatase and intestinal alkaline phosphatase in various human cell lines.[27] In addition, PLAP is one of the first proteins discovered to be ectopically expressed by cancer cells, leading to the concept that dysregulation of embryonic genes plays a significant role in the cancer process.[28] During the last 30 years, many clinical observations on PLAP and its use as a tumor marker have been made.[29−32] Thus, this hydrolytic enzyme represents an attractive target that is likely to play a role in the diagnosis and therapy of cancer.

In structure-based drug design, in silico docking is playing an increasing role as an efficient tool. However, docking of drugs to metalloenzymes remains a challenge due to the multiple coordination geometries of metals and the lack of appropriate force-field parameters to simulate metal−ligand interactions. For instance, zinc is found generally to be four-coordinated with a tetrahedral geometry, but five- and six-coordinated geometries, such as octahedral, square-base pyramidal, and trigonal bipyramidal, are also observed in metalloenzymes, especially in zinc metalloproteinases.[33] Modeling of zinc−ligand interactions with such multifarious coordination is considered problematic. Several high-quality, metal-associated, ligand−protein docking examples have recently been deduced from protein structures and ligand−protein reaction mechanisms.[34,35]

We searched for AP structures in the Protein Data Bank (PDB) and found that the X-ray crystal structure of human placental AP (PLAP) has been elucidated with 1.8 Å resolution (PDB code: 1EW2).[22] In these studies, comparison of the crystal structure of this hydrolytic enzyme with that of *Escherichia coli* revealed that only the overall features of the enzyme have been conserved: the surface is deeply mutated with 8% residues in

Table 1. Structure of a Series of Iodinated/Noniodinated Quinazolinone Analogues and Their Predicted ΔG and K_i

compd	R$_1$	R$_2$		ΔG^a (kcal/mol)	K_i^b (T = 298.15 K)
	I	OPO$_3^=$	OH		
8	6-	2'-	-	−12.86	3.77 × 10^{-10}
32	6-	-	2'-	-	-
9	-	2'-	-	−11.46	3.97 × 10^{-9}
10	6-	3'-	-	−12.15	1.23 × 10^{-9}
11	-	3'-	-	−10.96	9.26 × 10^{-9}
12	6-	4'-	-	−11.51	3.64 × 10^{-9}
13	-	4'-	-	−10.24	3.10 × 10^{-8}
14	6-	2',6'-	-	−12.10	1.35 × 10^{-9}
15	6-	3',5'-	-	−13.05	2.07 × 10^{-10}
16	6-	2',5'-	-	−12.75	4.49 × 10^{-10}
17	6-	2',4',6'-	-	−12.49	7.05 × 10^{-10}
18	6-	2',3',4'-	-	−12.21	1.04 × 10^{-9}
19	6-	2',3',5'-	-	−12.28	9.20 × 10^{-10}
20	6-	2',3',6'-	-	−11.85	1.91 × 10^{-9}
21	6-	2',4',5'-	-	−12.34	8.31 × 10^{-10}
22	6-	3',4',5'-	-	−12.17	1.11 × 10^{-9}
23	-	2',4'-	-	−11.55	3.40 × 10^{-9}
24	5-	2',4'-	-	−13.35	1.65 × 10^{-10}
25	5-	2',5'-	-	−12.65	4.92 × 10^{-10}
26	5-	2',6'-	-	−11.89	1.78 × 10^{-9}
27	5-	3',5'-	-	−12.71	4.45 × 10^{-10}
28	7-	2',4'-	-	−12.38	8.35 × 10^{-10}
29	8-	2',4'-	-	−12.24	1.06 × 10^{-9}
4, 6	6-	2',4'-	-	−13.77	8.96 × 10^{-11}
2, 7	6-	-	2',4'-	-	-
30	6-	2'-	4'-	−13.11	2.47 × 10^{-10}
31	6-	4'-	2'-	−11.74	2.31 × 10^{-9}

^{a} Binding free energy. ^{b} Inhibition constant.

common, and in the active site, only those residues strictly necessary for performing the catalysis have been retained. However, zinc and magnesium ions are still observed in the active site, indicating their indispensable roles in the catalytic reaction mechanism.

Previously, we had identified, synthesized, and characterized ammonium 2-(2'-phosphoryloxyphenyl)-6-[^{127}I/^{125}I]iodo-4-(*3H*)-quinazolinone (^{127}I/^{125}IQ$_{2-P}$, **8**) a derivative that is hydrolyzed in vitro to 2-(2'-hydroxyphenyl)-6-[^{127}I/^{125}I]iodo-4-(*3H*)-quinazolinone (^{127}I/^{125}IQ$_{2-OH}$, **32**) in the presence of AP.[14] Furthermore, we had shown that in vitro incubation of **8** with several human and mouse tumor-cell lines leads to the efficient and rapid formation of **32**, whereas the compound is minimally hydrolyzed in the presence of normal mouse liver, spleen, kidney, and muscle cells.[15−17] In conjunction with our efforts to develop novel radiolabeled prodrugs that are based on an analysis of the PLAP crystal structure and the ligand−PLAP reaction mechanism, the Lamarckian Genetic Algorithm (AutoDock 3.0)[36] has been explored (i) to model the interaction−binding between a series of radioiodinated quinazolinone derivatives and PLAP, and (ii) to assess the effects of structural modification of iodinated quinazolinone derivatives. Various analogues of the original quinazolinone derivative, in which the positions and numbers of the phosphoryloxy group and iodine atom were altered (Table 1), have been generated in silico, and the derivatives have been docked onto PLAP. Each prodrug−PLAP complex has been minimized, and the free binding energy

($\Delta G_{binding}$) and inhibition constant (K_i) have been estimated and compared. The approach can thus predict the reactivity of new radioiodinated quinazolinone derivatives *prior to* their chemical synthesis and as such aims to guide in the design and selection of radiolabeled quinazolinone analogues for use in the noninvasive radiodiagnosis ($^{123}I/^{124}I/^{131}I$) and therapy ($^{131}I/^{211}At$) of cancer. To our knowledge, few in silico based radiopharmaceutical development methods have been described.[37] We believe our studies provide a good example of computer-assisted development of radiopharmaceuticals for targeting cancer. Since this method could dramatically save time and money, it should advance the fields of nuclear medicine and cancer research in general.

Results and Discussion

Modeling of PLAP and Ligands. The docking model presented below relies substantially on the analysis of the active-site architecture of PLAP. Although this site has been described,[22] precise analysis is summarized here from the docking-dataset point of view. The active site of PLAP is considered to be Ser92, the metal triplet (two Zn^{2+} and one Mg^{2+}) and its substrate (phosphate), as well as Arg166 and other amino acids in the immediate vicinity (Figure 2A). The structure suggests the presence of a hydrophilic pocket in the active site, which indicates that the molecular mechanism underlying the interaction of phosphate with PLAP involves Glu429 and Arg166. The participation of these two amino acids allows precise description of this pocket, which probably stabilizes the hydrophilic moiety of the substrate. Glu429 is located at the entrance to the cleft where its Oϵ1 oxygen interacts with His320 Nδ. In turn, His320 Nϵ interacts with Zn1. Thus, the network consisting of Glu429−His320−Zn1−PO$_4$ may affect the hydrolysis of the phosphoryloxy moiety. This moiety interacts through hydrogen-bond binding with the His320, His432, Arg166, and Ser92 residues in PLAP. In addition to the tightly bound phosphoryloxy moiety, several water molecules are located within the active site (Figures 2A, 2D, 2E), and they form an extensive hydrogen-bonding network. Zn1 is hexacoordinated by the imidazole nitrogen atoms of His320 and His432, both carboxyl oxygens of Asp316 and two of the phosphate oxygens with an average metal−ligand distance of 2.48 Å. The polyhedron around Zn1 can be best described as trigonal bipyramidal with Zn1 occupying the apexes (Figure 2B). Zn2 is pentacoordinated by one of the carboxyl oxygens of Asp357 and two of the carboxyl oxygens of Asp42, the hydroxyl of Ser92, and one of the phosphate oxygens (Figure 2C). The average metal−ligand distance is 2.4 Å. Mg coordination can be described as a slightly distorted hexahedron, with the second carboxyl oxygen of Asp42, one of the carboxyl oxygens of Glu311, the hydroxyl of Ser155, and three water molecules (Wat1, Wat110, Wat421) completing the hexahedron (Figure 2D). The average Mg−O distance is 2.4 Å. Moreover, the three metals, two Zn^{2+} (referred as Zn1 and Zn2) and one Mg^{2+} are close in space: $d(Zn1-Zn2) = 4.0$ Å, $d(Zn2-Mg) = 4.8$ Å, and $d(Zn1-Mg) = 7.0$ Å. Phosphate is coordinated to the two nitrogen atoms held by the guanidinium group of Arg166 and the hydroxyl and amide of Ser92 (Figure 2E). The phosphate is further hydrogen-bonded to two water molecules (Wat71 and Wat315) and to another water molecule (Wat110) that is coordinated to Mg. Thus, the phosphate moiety is very closely associated with all three metals: it bridges Zn1 and Zn2 and is hydrogen bonded to Wat110 (coordinating Mg). The amino acid residues (especially catalytic Ser92), the metal triplet (especially Zn1), and several water molecules are considered to be the core of the active site
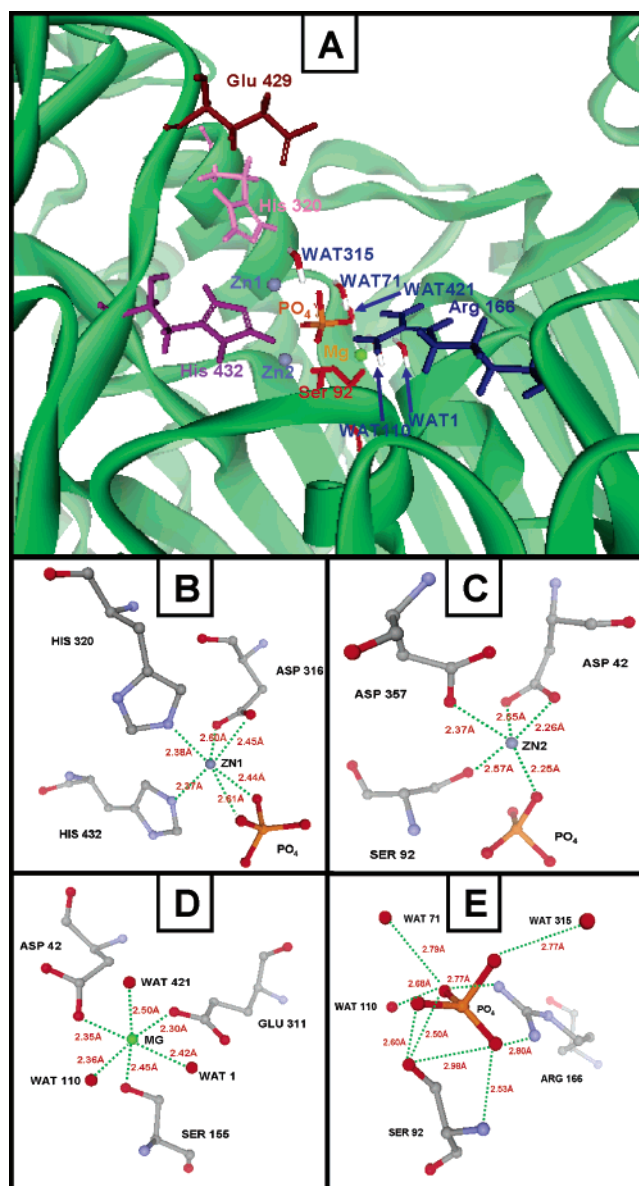

Figure 2. In silico modeling of PLAP. (A) Schematic representation of active site of PLAP crystal structure. PLAP (green) is in solid ribbon representation. Amino acid residues, phosphate, and Wat1, Wat71, Wat110, Wat315, Wat421 of PLAP in active site are in stick representation: Glu429 (brown), His320 (magenta), His432 (purple), Arg166 (dark blue), Ser92 (red), phosphorus (ochre), oxygen (red), hydrogen (white). Metal ions are in ball representation: Zn (blue-gray), Mg (light green). (B) Interactions of Zn1 with adjacent amino acid residues and phosphate. (C) Interactions of Zn2 with adjacent amino acid residues and phosphate. (D) Interactions of Mg with adjacent amino acid residues and water molecules. (E) Interactions of phosphate with adjacent amino acid residues and water molecules. These figures are drawn with DSViewPro and Insight II (Accelrys).

and have been shown to participate in PLAP-mediated hydrolysis of phosphoryloxy groups.[22]

Docking of PLAP and Ligands. Since the crystal structure of PLAP has been identified, PLAP-structure-based drug design is possible in developing new PLAP ligands. To provide the rapid evaluation of binding constants for PLAP, molecular docking studies, which are widely applied in structure-based drug design, have been performed. Although many different docking programs are applicable, no energy function is available for metalloproteins such as PLAP, which has three metal ions

in its active site. However, the use of an appropriately modified empirical scoring function is significantly less demanding on computational resources and thus allows the prompt evaluation of a large number of ligands. To validate the Zn parameters for use in AutoDock calculations, we started our docking study with **8** (structure shown in Table 1), a quinazolinone derivative that has already been identified, characterized, and shown to be hydrolyzed readily to **32** when incubated in the presence of AP.[14,15,17] The findings in one of these studies[15] indicate that **8** docks favorably into the active site of PLAP ($\Delta G_{binding} = -12.86$ kcal/mol). All 50 docking poses are clustered within 0.5 Å root-mean-square deviation (rmsd), indicating a strong consensus for a single binding mode. Along the active site, the quinazolinone moiety packs in the upper cleft of the binding pocket and the iodine atom poses against the pocket. The phosphorus group of **8** drops completely into the bottom of the binding pocket and faces the metal triplet. The average Zn1–ligand distance is 2.45 Å. Similarly to the binding pose of phosphate in the PLAP crystal structure, the phosphorus group of **8** bonds through hydrogen with amino acid residues in the active site, especially with the catalytic amino acid Ser92. The results also demonstrate that the parameters set for AutoDock simulations are reasonable and suitable for assessing the interaction of iodoquinazolinone analogues with PLAP.

Encouraged by this study, we have applied similar AutoDock parameters to subsequent docking studies with a series of iodinated quinazolinone derivatives and PLAP to assess the effects of structural modification. As shown in Table 1, the investigations of binding-affinity effects are focused on two areas: (i) the presence of the iodine atom and its position on the quinazolinone ring, (ii) the position and the number of phosphate groups in the benzene ring. First, we examined the mono-substituted phosphate group and its position in the benzene ring with the iodine atom fixed in the 6-position on the quinazolinone ring and observed that the binding affinities change slightly with the position of the phosphate group. The ortho-phosphate compound has the highest binding affinity compared with meta- and para-phosphate compounds, most likely because the carbonyl group of quinazolinone can more easily form hydrogen bonds with an adjacent amino acid in the active site and the ortho-phosphate group can drop into the bottom of the binding pocket. In addition, the absence of the iodine atom dramatically decreases the binding affinity (comparison of **8**–**13** in Table 1), indicating that the electronic potential of the iodine atom is vital for the interaction of quinazolinone derivatives with PLAP. Second, we studied multi-phosphate-substituted groups and their positions in the benzene ring with the presence of the iodine atom in the 6-position and observed that, with an increase in number of phosphates substituted in the benzene ring, the binding affinity of prodrugs with PLAP is enhanced. Generally, the binding affinities of double- and triple-phosphate-substituted compounds are higher than those of single-phosphate-substituted compounds (Table 1). Among the multi-phosphate-substituted molecules, the docking results indicate that at least one of the phosphate groups drops into the bottom of the binding pocket and interacts with the catalytic amino acid Ser92 and the metal triplet, and the remaining phosphate(s) have hydrogen bonds with adjacent amino acids and increase the binding affinity. However, the triple-phosphate-substituted compound does not have a significant increase of binding affinity (comparison of **4**, **14**–**22** in Table 1) which indicates that the size of the binding pocket likely accommodates a double-phosphate substituent, and an additional phosphate may cause steric effects and make the

Scheme 1

4 (*IQ$_{2-P, 4-P}$): *I = 127
6 (*IQ$_{2-P, 4-P}$): *I = 125

2 (*IQ$_{2-OH, 4-OH}$): *I = 127
7 (*IQ$_{2-OH, 4-OH}$): *I = 125
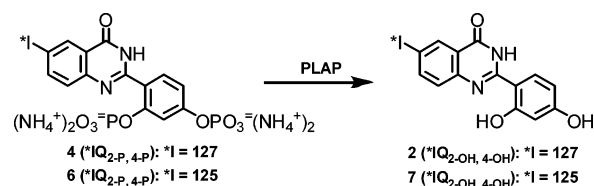
binding less favorable. Moreover, among double-phosphate-substituted compounds with the iodine atom in the 6-position of the quinazolinone ring, the 2′,4′-diphosphate-substituted demonstrates the highest binding affinity (comparison of **4**, **14**–**16** in Table 1). Finally, after in silico identification of the favorable 2′,4′-diphosphate substituents in the benzene ring, we docked into PLAP several compounds with 2′,4′-diphosphate substituents and with different positions of the iodine atom or without the iodine atom. A comparison of **4**, **23**, **24**, **28**, and **29** (Table 1) confirms that the presence of the iodine atom is crucial for binding, mainly due to the contribution of its electronic potential. Compound **24**, with the iodine atom in the 5-positon and 2′,4′-diphosphate substituents, has reasonably high binding affinity compared with **4**. In order to assess thoroughly the effects of structural modification, we studied the docking of PLAP with **25**–**27**, where the iodine atoms are located in the 5-position of the quinazolinone moiety and different combinations of diphosphate substituents are located in the phenyl moiety. None of these compounds has higher binding affinity than **4** (comparison of **4**, **25**–**27** in Table 1). In summary, for the iodine atom the 6-position of the quinazolinone ring is more likely favorable for binding compared with the other positions, and the 2′,4′-diphosphate-substituted compound with iodine atom in the 6-position of the quinazolinone ring (**4**, IQ$_{2-P,4-P}$) has the highest binding affinity, thus implying that **4** fits the binding pocket of PLAP most satisfactorily and is potentially the best substrate among the analogues.

The best docked pose of **4** with PLAP is shown in Figure 3A. The docked structure has multiple interactions with the metal ions, the residues, and the water molecules within the active site of PLAP. In the general docking profile, the quinazolinone moiety packs in the up cleft of the binding pocket and the iodine atom poses against the pocket. To be positioned in the middle of the binding pocket, the benzene ring adopts noncoplanar conformation with the quinazolinone ring, and the dihedral angle between them is 38.67°. The para-phosphate group of **4** twists slightly ($\angle_{P-O-C} = 124.15°$) to drop completely into the bottom of the binding pocket and to face the metal triplet. Similarly to the binding pose of phosphate in the PLAP crystal structure, the para-phosphate group forms hydrogen bonds with amino acid residues in the active site (Figure 3B). In addition to forming a salt bridge with the guanidino group of Arg166, the para-phosphate group of **4** is also capable of contacting His432 Nϵ2. Most important, the phosphorus group of **4** bonds through a hydrogen atom with the catalytic amino acid Ser92, and the distance between the oxygen of phosphate and the NH group in the side chain of Ser92 is 2.06 Å, indicating that **4** interacts easily with Ser92 for dephosphorylation. Moreover, the interaction of the para-phosphate group of **4** with metal ions and the water network, particularly with Zn1 and Wat315, is observed (Figure 3C). The average distance among the interactions of Zn1–Wat315–para-phosphate is 2.8 Å (Figure 3C), indicating that Zn1 and Wat315 play an important role in the hydrolytic mechanism. The second phosphate in the ortho-position forms hydrogen bonds with the guanidino group of Arg150, and the oxygen atom of the
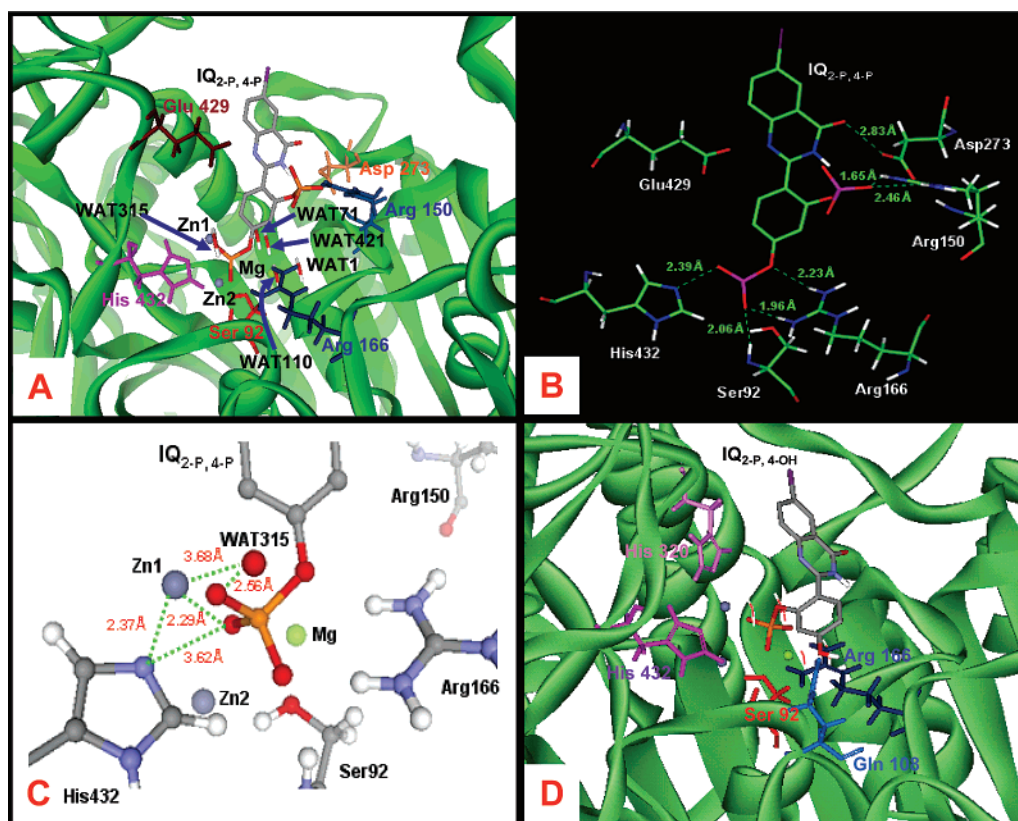
Figure 3. Docking of compounds **4** and **30** with PLAP. (**A**) Schematic representation of docking of **4** with PLAP crystal structure. PLAP (green) is in solid ribbon representation. Amino acid residues, phosphate, and Wat1, Wat71, Wat110, Wat315, Wat421 of PLAP in active site are in stick representation: Glu429 (brown), His432 (magenta), Arg166 (dark blue), Ser92 (red), Arg150 (light blue), Asp273 (orange), phosphorus (ochre), oxygen (red), hydrogen (white). Metal ions are in ball representation: Zn (blue-gray), Mg (light green). (**B**) Hydrogen bonds of **4** with interacting amino acid residues in PLAP. (**C**) Bonds of para-phosphate of **4** with Zn1, adjacent amino acid residues, and Wat315. (**D**) Overall profile of docking results of **30** with PLAP crystal structure. PLAP (green) is in solid ribbon representation. Amino acid residues and phosphate in active site are in stick representation: His320 (magenta), His432 (purple), Arg166 (dark blue), Ser92 (red), Gln108 (light blue), phosphorus (ochre), oxygen (red), hydrogen (white). Metal ions are in ball representation: Zn (blue-gray), Mg (light green). These figures are prepared with DSViewPro and Insight II (Accelrys).

Scheme 2[a]
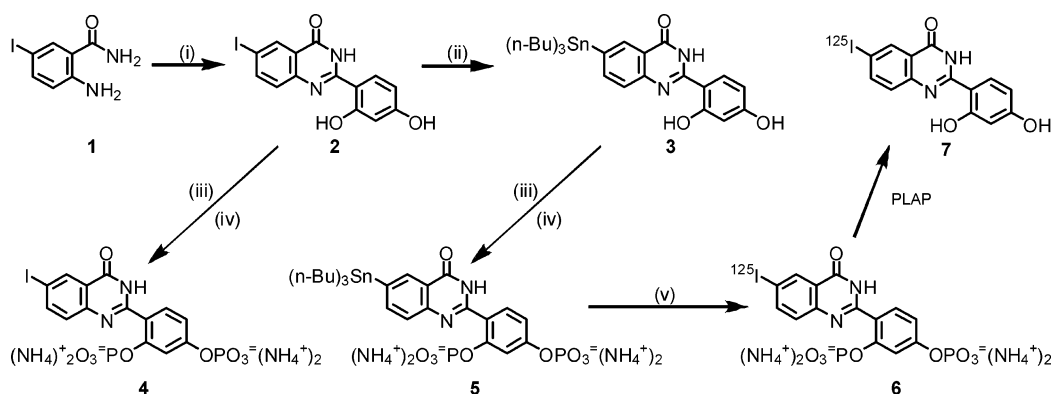
[a] Reagents and conditions: (i) 2,4-dihydroxybenzaldehyde, *p*-toluenesulfonic acid; (ii) hexa-*n*-butylditin/palladium(0)/dioxane, reflux; (iii) phosphorus oxychloride/benzene/0 °C; (iv) 28% aqueous ammonium hydroxide; (v) Na^{125}I/Iodogen.

carbonyl group in the quinazolinone moiety accepts a hydrogen bond from Asp273, both of these further tightening the binding of **4** with PLAP (Figure 3B). Fifty genetic algorithm runs of the docking of **4** with PLAP suggest that the para-phosphate group is more favorable for hydrolysis than the ortho-phosphate group, whose position is less close to the metal ions, the catalytic residues, and the mediated water molecules.

To further investigate the hydrolytic mechanism of **4** with PLAP, we simulated the interaction of IQ$_{2-P,4-OH}$ (**30**), the possible intermediate hydrolytic product of **4** with PLAP (Figure 3D). The docking of **30** also leads to very positive results (Table

1). Similarly to the binding pose of the para-phosphate of **4** with PLAP, the ortho-phosphate group of **30** maintains interactions with the metal ions, the catalytic residues, and the mediated water molecules in the active site (Figure 3D), suggesting that the ortho-phosphate group is also capable of being hydrolyzed after the hydrolysis of para-phosphate. In addition, we attempted to dock **31** (IQ$_{2-OH,4-P}$) into PLAP to explore the possibility of **31** as the intermediate hydrolytic product of **4** with PLAP. The docking studies demonstrate that **31** has significantly lower binding affinity with PLAP than does **30** (Table 1), indicating that **31** is unlikely to be the PLAP substrate. Thus the
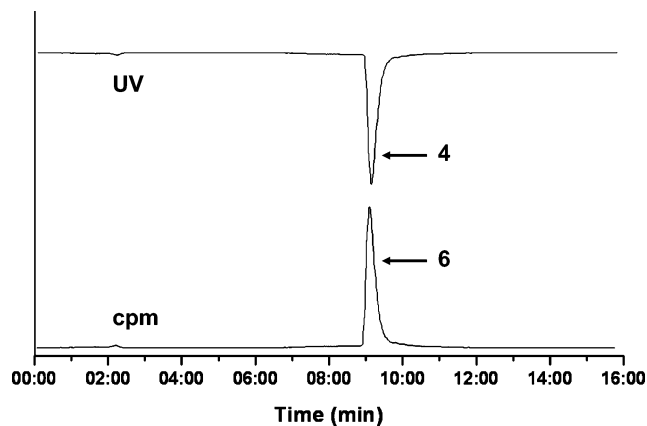
Figure 4. HPLC profile of **4** and **6**. Column: ZORBAX SB-C$_{18}$ (5 μm, 9.4 × 250 mm); eluents: A, 0.05 mol/L phosphate buffer (pH 2.5), B, methanol; gradient of 0% to 100% B over 16 min, flow rate, 3 mL/min; detector, 254 nm; t_R, 9.08 min.

intermediate hydrolytic product of **4** is more likely to be **30** than **31**. We hypothesize that the hydrolytic mechanism of **4** consists of two events. First, the para-phosphate group drops into the bottom of the catalytic binding site and is hydrolyzed to **30**. With the release of the first phosphate group, the benzene ring rotates and the second phosphate group in the ortho-position faces the catalytic binding site and the para-hydroxyl group further tightens the binding pose of **30**. Since the rotation of a single carbon−carbon bond between the quinazolinone and benzene rings requires minimal energy, the second hydrolytic procedure (i.e., the further hydrolysis of **30**) seems to be highly possible and must be very prompt. This suggests that under certain circumstances, the hydrolytic product of **4** may in reality be IQ$_{2-OH,4-OH}$ (**2**) rather than **30** (Scheme 1).

Llinas et al.[38] recently have reported new structural studies of PLAP in complex with functional ligands. Among their findings, a remote peripheral site located 28 Å from the active site has been observed to have potential for the interaction of ligands with PLAP. Further docking explorations of our designed analogues in this new site are currently underway.

Synthesis and Chemical Characterization. Guided by the docking results, we synthesized and characterized prodrug ammonium 2-(2′,4′-diphosphoryloxyphenyl)-6-iodo-4-(*3H*)-quinazolinone (^{127}IQ$_{2-P,4-P}$ (**4**)/^{125}IQ$_{2-P,4-P}$ (**6**)) and drug 2-(2′,4′-dihydroxyphenyl)-6-[^{127}I/^{125}I]iodo-4-(*3H*)-quinazolinone (^{127}IQ$_{2-OH,4-OH}$ (**2**)/^{125}IQ$_{2-OH,4-OH}$ (**7**)) (Schemes 1 and 2). Radiolabeled quinazolinone-derivative **6** co-injected into the HPLC with nonradioactive quinazolinone-derivative **4** showed a single radioactive peak that matched the retention-time value of **4** (Figure 4). HPLC analysis also indicated the radiochemical yield for **6** was 96% and the radiochemical purity was greater than 98% (Figure 4). We attempted also to synthesize the monophosphate compound substituted in either the ortho-position or the para-position (i.e., **30** or **31**) through the phosphorylation of **2**. Our efforts were unsuccessful, a circumstance that may be due to the similar reaction function of the two hydroxyl groups of **2** in the benzene ring.

PLAP-Dependent Conversion of 4 to 2. When **4**, a nonfluorescent compound, was incubated with PLAP and the kinetics of hydrolysis were followed with a luminescence spectrometer, a rapid increase in fluorescence intensity (excitation at 340 nm; emission at 466.05 nm) (Figure 5, top) was observed, demonstrating the hydrolysis of **4** and the formation of **2** (Scheme 1). Analysis of the data indicates the PLAP-dependent disappearance of **4** (or the appearance of **2**) is biphasic
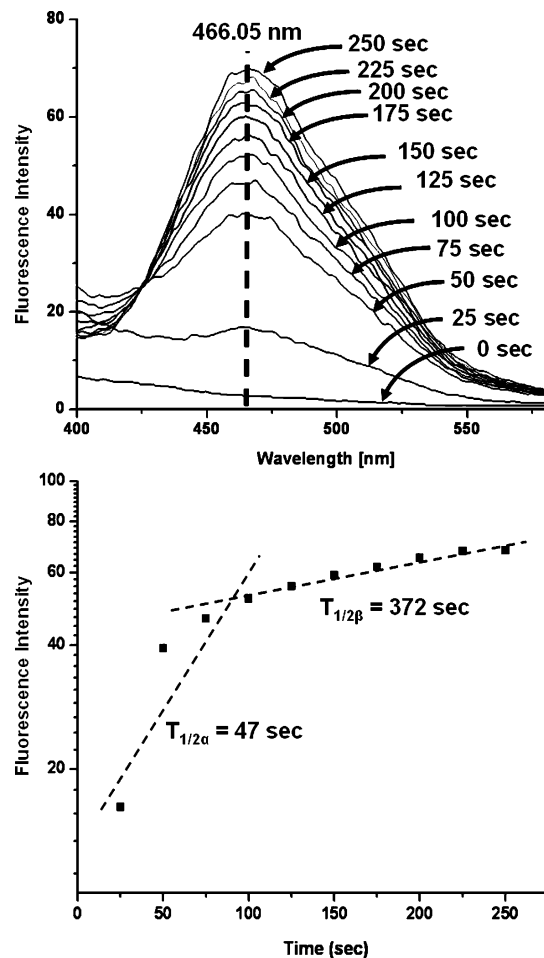

Figure 5. Kinetics of PLAP-based hydrolysis of **4** at 37 °C. (Top) Change in fluorescence intensity of **4** at 466.05 nm as function of time (time interval 25 s). (Bottom) Linear fit for calculating slopes and corresponding $T_{1/2\alpha}$ and $T_{1/2\beta}$.

with a $T_{1/2\alpha}$ of 47 s and $T_{1/2\beta}$ of 372 s (Figure 5, bottom); therefore, the initial hydrolysis of prodrug **4** by PLAP is prompt.

To assess the kinetics of PLAP-base hydrolysis, a Lineweaver−Burk plot was constructed (see Supporting Information). The Michaelis−Menten constant of PLAP (K_m) is 1.08 × 10^{-4} mol/L and the maximum velocity (V_{max}) is 1.41 × 10^{-5} mol/L/min, obtained by extrapolating the straight line to its intercepts on the *x* and *y* axes.

PLAP-Dependent Conversion of 6 to 7. HPLC analysis was utilized to characterize the water-soluble radioiodinated prodrug **6** and confirm its PLAP-dependent hydrolysis to radioiodinated drug **7** (Scheme 1). When **6** was incubated with various concentrations of PLAP, the peak of substrate **6** (t_R 9.08 min) disappeared as a function of increasing PLAP concentration (Figure 6A). Simultaneously a new peak appeared at t_R 10.52 min, which matched the retention-time value of **2**. The 10-min incubation of **6** with various concentrations of PLAP led to its conversion to **7**, and with 10 Units/μL PLAP, **6** was completely converted to **7**. The percentage conversions of **6** to **7** were determined after integration of the peak area of **7**. A plot of PLAP concentration (abscissa) versus formation of **7** (ordinate) furnishes a sigmoidal line (IC$_{50}$ = 78 000 Units/L) that indicates that the minimum PLAP concentration needed to hydrolyze **6** is ≥2000 Units/L (Figure 6B), a value much higher than the 500 Units/L found in the blood of cancer patients.[30,39−42] Consequently, prodrug **6** is not expected to be hydrolyzed following its intravenous injection into patients.
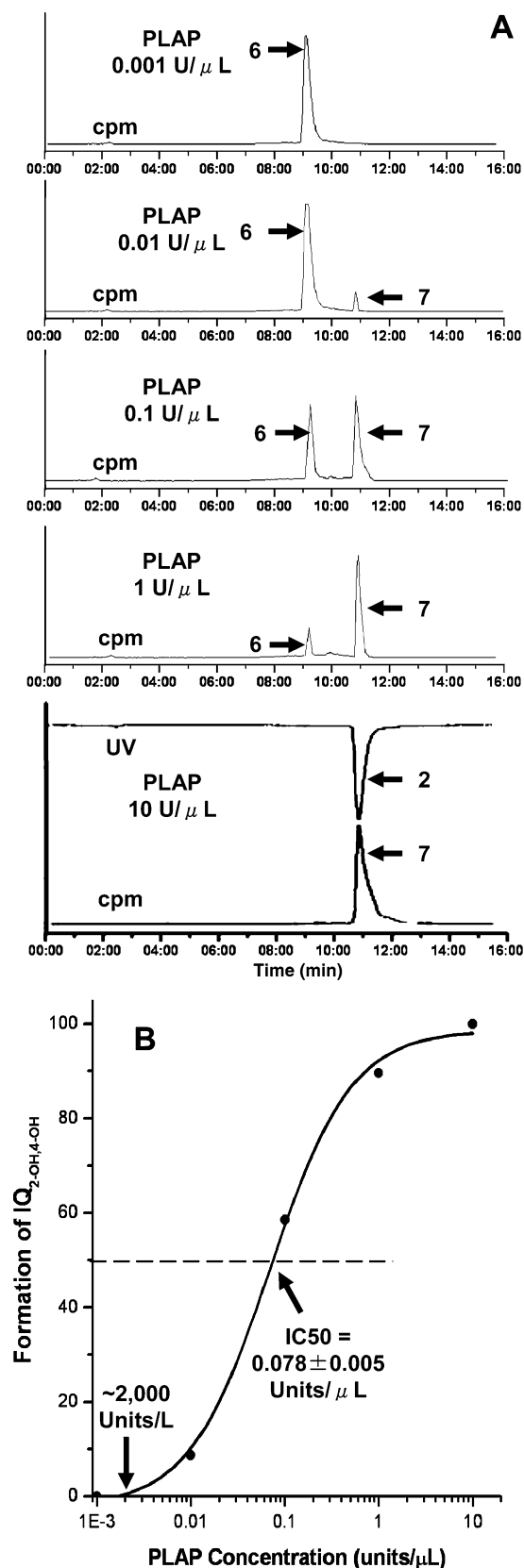
Figure 6. Kinetics of PLAP-mediated hydrolysis of **6** to **7** determined by HPLC analysis. Incubation at 37 °C, pH 7.4, for 10 min.
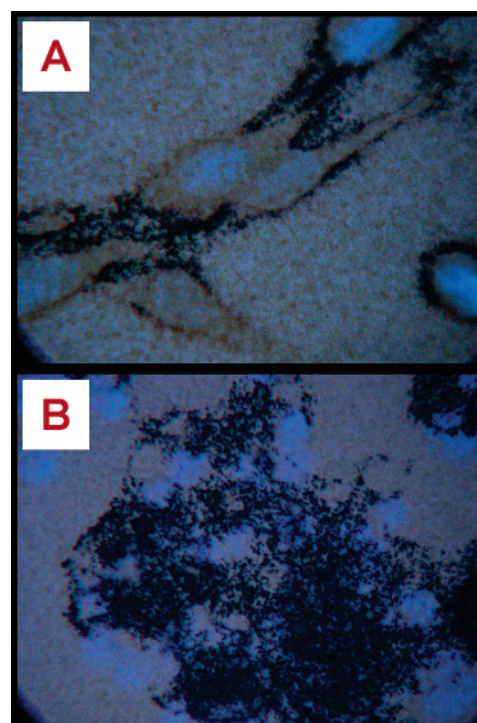

Figure 7. Autoradiography of preparations containing human cancer cells and **6**. TE671 (A) and OVCAR3 (B) human tumor cells incubated in vitro for 24 h with **6**, showing hydrolysis of prodrug and precipitation of **7** (intense grains associated with cell membranes). Cell nuclei counterstained blue with DAPI.
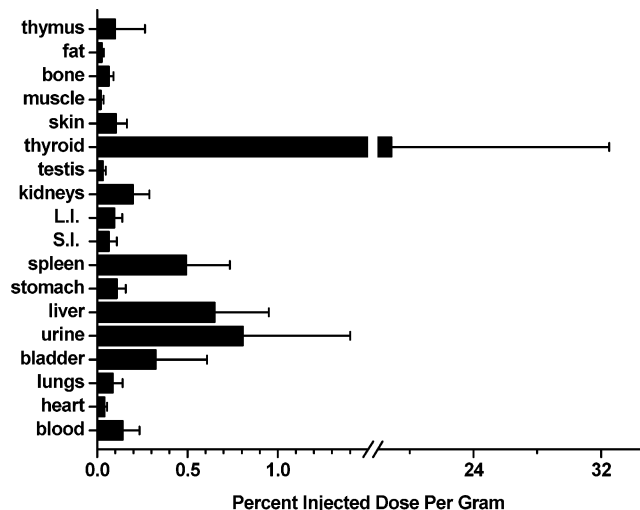

Figure 8. Biodistribution of **6** in normal mice. Percentage injected dose per gram (% ID/g) calculated for tissues, organs, and fluids 24 h post iv injection of **6**.

Solubility Determination for 4 and 2. To assess the solubility of **4** and **2**, the recently described radiotracer analysis method was applied.[43] The solubility of **4** is 4.35 ± 0.14 mg/mL, whereas that of **2** is 9.68 ± 0.22 ng/mL. Since the EMCIT approach requires that the quinazolinone analogue produced after enzymatic hydrolysis be highly water-insoluble and **2** is ∼2 million times less soluble than **4**, the newly synthesized prodrug is likely to precipitate and be entrapped within solid tumors, thus validating the EMCIT principle.

Examination by Autoradiography of Hydrolysis of 6 Incubated with Human Tumor Cells. Autoradiography was used to verify the hydrolysis of water-soluble **6** to water-insoluble **7** by mammalian tumor cells that overexpress AP. The incubation of TE671 (human rhabdomyosarcoma) and OVCAR3 (human ovarian carcinoma) cells with **6** led to formation of large areas of black grains, which were strongly and irreversibly bound to the cell surface (Figure 7).

Biodistribution of 6 in Normal Mice. Twenty-four hours after the administration of **6** to normal mice, biodistribution of the prodrug was determined by calculating the percentage injected dose per gram tissue/organ (% ID/g). The data (Figure 8) indicate that (i) the prodrug is cleared quickly from blood ($0.14 \pm 0.09\%$ ID/g), (ii) some radioactivity is present in the thyroid ($18.85 \pm 13.65\%$ ID/g), (iii) minimal amounts of radioactivity are detected in liver and spleen ($0.65 \pm 0.30\%$ ID/g and $0.49 \pm 0.24\%$ ID/g, respectively), and (iv) very little radioactivity is present in other organs and tissues ($<0.2\%$ ID/g). These findings suggest that (i) **6** and/or its breakdown/hydrolysis product(s) are not taken up, hydrolyzed, or retained by most normal tissues and are rapidly excreted through the urinary system, and (ii) minimal dehalogenation of the compound occurs ($<0.1\%$ of the injected dose), as exemplified by the small amount of radioactivity within the thyroid.

Conclusion

A rational approach to the design and synthesis of novel radiolabeled prodrugs is being advanced. The Lamarckian genetic algorithm has been employed to model the interaction—binding of a series of quinazolinone analogues with PLAP. The procedures offer guidance in the design of iodinated quinazolinone derivatives for use in noninvasive radiodiagnosis (^{123}I/[124]I/^{131}I) and therapy (^{131}I/[211]At) of cancer and aid in the selection of agents that are well-suited to EMCIT. The approach is general and can be applied to the development of other diagnostic and therapeutic radiopharmaceuticals for specific enzyme and other macromolecular targets. The further evaluation of these compounds for radioimaging and radiotherapy is currently in progress in preclinical animal models.

Experimental Section

Computational Methodology. Dataset of PLAP and Ligands. Three-dimensional coordinates of the PLAP structure were obtained from the PDB (code 1EW2).[22] The PLAP dimer structure was produced according to the symmetry of atoms coordination. The repair of missing atoms within residues was performed in Swiss-Pdb viewer.[44] The hetero atoms including cofactors and phosphate were removed. Two zinc ions and one magnesium ion at the active site were retained. All bound water molecules except five (WAT1, WAT71, WAT110, WAT315, WAT421), involved in interactions between the phosphate and PLAP, were discarded. Polar hydrogens were added and the united partial charges for PLAP atoms were taken from the AMBER force field[45] of the Insight II package.[46] Atomic solvation parameters were assigned to PLAP using the AutoDock module AddSol. All the residues and charges were visually inspected to ensure consistency and reasonableness. All histidines were assigned as singly protonated. As a result, two zinc-coordinated histidines were protonated on Hδ, whereas other histidines were protonated on Hϵ. The amino-acid side chains of arginine, lysine, aspartate, and glutamate residues were treated as ionized. CAChe molecular modeling software[47] was employed to build the structures of all ligands. To explore the possible low-energy conformations, the ligand structures were energy-minimized by applying the PM5 method in the MOPAC package. The partial atomic charges were calculated and all partial charges were further modified using the AutoDockTools package so that the charges of the nonpolar hydrogen atoms were assigned to the atom to which the hydrogen was attached. All ligands appeared in the charged form, i.e., the phosphates were deprotonated. All torsion angles of the ligands to be explored during molecular docking were defined.

Docking Protocol of PLAP and Ligands. The AutoDock 3.0 program[36] was used to perform automated molecular docking. The Lamarckian genetic algorithm (LGA) was applied to model the interaction—binding between PLAP and the quinazolinone analogues shown in Table 1. In the case of molecular docking, the LGA describes the relationship between a ligand and a protein by the translation, orientation, and conformation of the ligand. These are the state variables of the ligand, and each state variable is equivalent to a gene. The state of the ligand corresponds to the genotype, and its atomic coordinates to the phenotype. In the Lamarckian model of genetics, environmental adaptations of an individual phenotype are reverse-transcribed into its genotype, becoming heritable traits. Each docking cycle or generation consists of a regimen of fitness evaluation, crossover, mutation, and selection. Thus, the final solution results in a ligand conformation finely tuned to the protein, whereas more poorly suited conformations are not inherited.

The docking area (active site) of PLAP was defined using the AutoDock module AutoGrid. The grid site was constrained to a 24.75 Å cubic space centered on the original phosphate in the crystal structure. The grid box included the entire binding site of PLAP and provided sufficient space for translational and rotational walk of the ligand. The LGA in AutoDock 3.0 was applied to search the conformational and orientational space of the quinazolinone derivative while keeping the PLAP structure rigid. Default parameters were used, except that the maximum number of energy evaluations was set to 1.5×10^6. Fifty runs were performed. For each of the 50 independent runs, a maximum number of 2.7×10^4 genetic algorithm operations were generated on a single population of 50 individuals. Operator weights for crossover, mutation, and elitism were default parameters, 0.80, 0.02, and 1, respectively. Metal ions are modeled in AutoDock by Amber force-field potentials. However, we selected $r = 1.1$ Å (zinc radius), $\epsilon = 0.25$ kcal/mol (well depth) and a charge of $+2.0e$ as zinc parameters.[48] From the simulated model, binding free energy and affinity constant were obtained, and the docked complex of quinazolinone derivative—PLAP was selected according to the criteria of interacting energies matched with geometric quality. Further energy minimization and geometric optimization were performed on the selected complex until there were no conflicts among the ligand, the metal ions, the water molecules, and PLAP. The obtained complex was utilized for structure analysis and reaction mechanism studies.

Binding Affinity Prediction. Based on the traditional molecular force-field model of interaction energy, a new score function at the level of the binding free energy was derived and adopted in the AutoDock 3.0 version.[36] The restriction of internal rotors, global rotation, and translation were modeled depending on the calculated number of torsion angles of the ligand. The total binding free energy was empirically calibrated based on the terms stated above and a set of coefficient factors, using a set of 30 structurally known protein—ligand complexes with experimentally determined binding constants. The new score function is sufficient to rank the ligands on level of binding affinity, binding free energy ($\Delta G_{binding}$ values), and the corresponding inhibition constant (K_i values). We applied this scoring approach to the iodinated quinazolinone analogues and PLAP and calculated the total binding free energy and inhibition constant for these complexes according to the algorithm in the AutoDock 3.0 program. Guided by the above docking results, **4** has been selected for further study.

Chemistry. Materials and Methods. All reagents were obtained from Sigma-Aldrich Chemical Co. and used without further purification. Carrier-free sodium [^{125}I]iodide was obtained from GE Healthcare Corporations. ^{1}H and ^{31}P NMR spectra were recorded on a Varian XL-200 spectrometer and the ^{13}C NMR spectrum was recorded on a Varian INOVA 500 MHz spectrometer. Analytical thin-layer chromatography (TLC) was carried out on Sigma-Aldrich silica gel plastic sheets. Column chromatography was used for the routine purification of reaction products. The column output was monitored by TLC. HPLC separations were performed on a reversed-phase ZORBAX SB—C$_{18}$ column, 9.4 × 250 mm (Agilent Technologies), at a flow rate of 3 mL/min. UV absorption (Waters 2487 detector, 254 nm) and γ-ray detection were used to analyze the eluates. Electrospray mass spectra were recorded on a Micromass Platform LCT mass analyzer. High-resolution mass spectrometry was performed on a Bruker Daltonics ApexII 3T

Fourier transform mass spectrometer. 2-Amino-5-iodobenzamide (**1**) was prepared as reported previously.[14]

Compound 2. 2-Amino-5-iodobenzamide (**1**) (1.834 g, 7.0 mmol, 1.0 equiv) and 2,4-dihydroxybenzaldehyde (1.16 g, 8.4 mmol, 1.2 equiv) were suspended in methanol (40 mL) and refluxed in the presence of catalytic amounts of *p*-toluenesulfonic acid (0.183 g, 10%) for 15 h (Scheme 2). After the reaction mixture was filtered and washed with cold methanol, **2** was obtained as a light-brown solid (2.18 g, 82%). ^{1}H NMR (200 MHz, DMSO-d_6) δ 10.30 (s, 1H), 8.36 (s, 1H), 8.10 (d, $J = 8.8$ Hz, 1H), 8.06 (d, $J = 8.4$ Hz, 1H), 7.48 (d, $J = 8.8$ Hz, 1H), 6.39 (d, $J = 8.4$ Hz, 1H), 6.35 (s, 1H); ^{13}C NMR (125 MHz, DMSO-d_6) δ 162.9, 162.6, 160.3, 154.4, 145.8, 143.3, 134.4, 129.4, 127.8, 122.0, 108.0, 105.2, 103.5, 90.7; ESI-HRMS m/z C$_{14}$H$_9$IN$_2$O$_3$ [M + H]$^+$ calcd, 380.9731; found, 380.9730.

2-(2′,4′-Dihydroxyphenyl)-6-tributylstannyl-4-(3H)-quinazolinone (3). To a stirred solution of **2** (0.57 g, 1.5 mmol, 1.0 equiv) in dioxane (20 mL) was added hexa-*n*-butylditin (1.82 g, 3.0 mmol, 2.0 equiv), followed by tetrakis(triphenylphosphine)palladium (17.0 mg, 0.015 mmol) as catalyst. The reaction mixture was refluxed for 6 h, and progress of the reaction was followed by silica gel TLC with petroleum ether:acetone (2:1) to test for the formation of a more nonpolar product. The solvent was evaporated, and the crude solid was purified on a silica gel column eluted with a stepwise gradient, starting with hexane followed by hexane:ethyl acetate (10:1). The solvent was removed to give a yellow solid **3** (0.56 g, 69%). ^{1}H NMR (200 MHz, DMSO-d_6) δ 10.26 (s, 1H), 8.18 (s, 1H), 8.09 (d, $J = 8.4$ Hz, 1H), 7.86 (d, $J = 8.2$ Hz, 1H), 7.61 (d, $J = 8.4$ Hz, 1H), 6.37 (d, $J = 8.2$ Hz, 1H), 6.34 (s, 1H), 1.52 (quintet, $J = 7.4$ Hz, 6H), 1.30 (sextet, $J = 7.4$ Hz, 6H), 1.10 (dd, $J = 8.4$ Hz, $J_{Sn-CH} = 52.0$ Hz, 6H), 0.85 (t, $J = 7.4$ Hz, 9H); ^{13}C NMR (125 MHz, DMSO-d_6) δ 162.9, 162.7, 161.7, 154.2, 146.2, 142.3, 139.8, 133.8, 129.1, 124.5, 119.7, 107.8, 105.2, 103.5, 28.7, 26.8, 13.5, 9.4; ESI-HRMS m/z C$_{26}$H$_{36}$N$_2$O$_3$Sn [M + H]$^+$ calcd, 545.1836; found, 545.1831.

Compound 4. A solution of pyridine (32.8 μL, 0.4 mmol, 2.0 equiv) in benzene (1.5 mL) was slowly added to a mixture of **2** (76 mg, 0.2 mmol, 1.0 equiv) and phosphorus oxychloride (0.55 mL, 6.0 mmol, 30.0 equiv) in benzene (1.5 mL) cooled to 0 °C. The mixture was stirred for 5 h at 0 °C. Subsequently ether (15 mL) was added. The solid was removed by filtration. The solvents were removed, and ether (15 mL) was added again. The remaining solids were removed, and the solvent was evaporated. The surplus of phosphorus oxychloride was removed in vacuum. Without further purification, ammonium hydroxide solution (28%, 0.28 mL) was added dropwise to the yellow residue at 0 °C until pH 7 was achieved. The solvent was evaporated, and a yellow solid was obtained. The crude product was redissolved in methanol:water (1:1) and purified on a Sephadex G-10 column using a stepwise gradient, starting with water followed by acetonitrile:water going from 50% to 80% acetonitrile. The solvent was evaporated under reduced pressure. A light-yellow solid **4** was obtained (105 mg, 86%). ^{1}H NMR (200 MHz, D$_2$O) δ 8.24 (s, 1H), 7.94 (d, $J = 8.8$ Hz, 1H), 7.76 (d, $J = 8.8$ Hz, 1H), 7.28 (d, $J = 8.8$ Hz, 1H), 7.18 (s, 1H), 7.06 (d, $J = 8.8$ Hz, 1H); ^{31}P NMR (D$_2$O, H$_3$PO$_4$ as external reference) δ 1.132, 1.547; ESI-HRMS m/z C$_{14}$H$_{11}$IN$_2$O$_9$P$_2$ [M + H]$^+$ calcd, 540.9063; found, 540.9059.

Ammonium 2-(2′,4′-Diphosphoryloxyphenyl)-6-tributylstannyl-4-(3H)-quinazolinone (5). To a stirred solution of **3** (108 mg, 0.2 mmol, 1.0 equiv) and phosphorus oxychloride (0.55 mL, 6.0 mmol, 30.0 equiv) in benzene (1.5 mL) cooled to 0 °C was added dropwise a solution of pyridine (32.8 μL, 0.4 mmol, 2.0 equiv) in benzene (1.5 mL). The mixture was stirred for 5 h at 0 °C. Subsequently ether (15 mL) was added. The remaining solids were removed, and the solvent was evaporated. The surplus of phosphorus oxychloride was removed in vacuum. Ammonium hydroxide solution (28%, 0.28 mL) was added dropwise to the yellow residue at 0 °C until pH 7 was attained. The solvent was evaporated, and a yellow solid was obtained. The crude product was redissolved in methanol:water (1:1) and purified on a Sephadex G-10 column using a stepwise gradient, starting with water, followed by acetonitrile:water going from 50% to 80% acetonitrile. The solvent was evaporated under reduced pressure. A light-yellow solid **5** was obtained (125 mg, 81%). ^{1}H NMR (200 MHz, D$_2$O) δ 8.15 (s, 1H), 7.84 (d, $J = 8.6$ Hz, 1H), 7.76 (d, $J = 8.6$ Hz, 1H), 7.54 (d, $J = 8.6$ Hz, 1H), 7.30 (s, 1H), 7.15 (d, $J = 8.6$ Hz, 1H), 1.39 (quintet, $J = 7.4$ Hz, 6H), 1.26 (sextet, $J = 7.4$ Hz, 6H), 1.14 (dd, $J = 8.4$ Hz, $J_{Sn-CH} = 52.0$ Hz, 6H), 0.73 (t, $J = 7.4$ Hz, 9H); ^{31}P NMR (D$_2$O, H$_3$PO$_4$ as external reference) δ 1.342, 1.764; ESI-HRMS m/z C$_{26}$H$_{38}$N$_2$O$_9$P$_2$Sn [M + H]$^+$ calcd, 705.1153; found, 705.1138.

Compound 6. To a reaction vial coated with 1,3,4,6-tetrachloro-3α,6α-diphenylglycouril (Iodogen) (10 μg) was added phosphate buffer (12 μL, 0.1 mol/L, pH 7.4), **5** (1 μL, 5 μg/μL DMSO solution), and 37−74 MBq Na^{125}I (in 2−4 μL 0.1 mol/L sodium hydroxide). After vortex mixing at ambient temperature for 4 min, the reaction solution was analyzed by HPLC on a reversed-phase ZORBAX SB−C$_{18}$ column using a linear gradient (3 mL/min) from 100% phase A (0.05 mol/L phosphate buffer, pH 2.5) to 100% phase B (methanol) in 16 min. Compound **6** eluted at 9.08 min (radiochemical yield 96%, radiochemical purity greater than 98%).

Solubility Determination for Prodrug 4 and Drug 2 Using Radiotracer Analysis Method.[43] Compound **6** (1.5 μL, 60 μCi/μL) in phosphate-buffered saline (0.1 mol/L, PBS) was added to a solution of **4** (200 μL, 0.5 μg/μL in DMSO). Various concentrations of radiotracer solution were prepared by adding different volumes of the original radiotracer solution (2 μL−12 μL, at increments of 2 μL) to vials containing distilled water, and the final volume in each vial was brought to 10 mL with distilled water. The vials were shaken for 10 min and then centrifuged for 30 min. The radioactivity of each supernatant was measured in a gamma counter. After calculating the ratio of radioactivity in solution to total radioactivity for each vial, the dissolved amount of **4** in solution in each vial was determined. Since (i) the iodine-125 and iodine-127 compounds have the same solubilities and are thus equally distributed in the DMSO−water solution, and (ii) the amount of nonradioactive compound (added in the DMSO solution) is known, the concentration of the compound in solution can be calculated and plotted as a function of the DMSO-to-water ratio. The water solubility of the compound is then determined by extrapolation of the linear fit of the data points to zero DMSO, i.e., the *y*-axis intercept when $x = 0$.[49]

The solubility of **2** in water was determined using the same methodology. The preparation of **7** was not through iododestannylation of **3**. Instead, **6** was incubated with PLAP (10 Units) at 37 °C for 10 min in Tris buffer (0.1 mol/L, pH 7.4), and its complete transformation to **7** was observed under such conditions (Figure 6). After obtaining **7**, a mixture of **2** and **7** was prepared and used as above to determine the solubility of **2**.

PLAP-Dependent Conversion of 4 to 2. To assess the kinetics of PLAP-based hydrolysis (i.e., conversion of **4** to **2**), **4** (80 μmol/L) was mixed with PLAP (40 Units) in Tris buffer (0.1 mol/L, pH 7.4) containing NaCl (50 mmol/L), MgCl$_2$ (10 mmol/L), and ZnCl$_2$ (0.1 mol/L), and the reaction was followed over time using a Perkin-Elmer LS50B luminescence spectrometer with excitation at 340 nm and emission at 466.05 nm. The fluorescence intensity at 466.05 nm was then plotted as a function of time, the linear portions of the data points are fitted, and the slope was used to calculate the half-life ($T_{1/2\alpha}$ and $T_{1/2\beta}$) for the disappearance of **4**.

To assess the kinetics further, **4** (60, 80, 90, 100, 110, 120 μmol/L) was mixed with PLAP (10 Units) in Tris buffer (pH 7.4), and the reactions were followed over time. A plot of reciprocal of the substrate concentration (prodrug **4**, abscissa) versus reciprocal of reaction velocity (ordinate) furnished a straight Lineweaver−Burk line with a slope equal to K_m/V_{max}. The *y* intercept of the line is $1/V_{max}$ and the *x* intercept is $-1/K_m$. K_m is the Michaelis−Menten constant of PLAP and V_{max} is the maximum velocity.

PLAP-Dependent Conversion of 6 to 7. Various concentrations of PLAP (0.001, 0.01, 0.1, 1, 10 Units/μL) were incubated with radioiodinated prodrug **6** (∼10 μCi/100 μL in 0.1 mol/L Tris buffer, pH 7.4) at 37 °C for 10 min. The samples were analyzed by HPLC, and the radioactivities were assessed. After integration of the peak area of the compounds on HPLC, the ratios of conversion of **6** to

7 were measured. Each experiment was repeated three times. Using the ORIGIN program,[49] a plot of PLAP concentration (abscissa) versus formation of **7** (ordinate) furnished a sigmoidal line from which the IC_{50} value as well as the minimal concentration of PLAP needed for any hydrolysis was calculated.

Examination by Autoradiography of Hydrolysis of 6 Incubated with Human Tumor Cells. Human OVCAR3 ovarian carcinoma cells (kindly provided by Thomas C. Hamilton, Fox Chase Cancer Center, Philadelphia) were cultured in RPMI 1640 supplemented with fetal bovine serum (10%). Human TE671 rhabdomyosarcoma cells (ATCC) were cultured in DMEM supplemented with fetal bovine serum (10%). The cells were grown in 75-cm^3 tissue-culture flasks and kept in a humidified atmosphere of 5% CO_2 at 37 °C, with the medium changed every other day. Logarithmically growing cells were trypsinized, suspended in medium, and seeded onto slides (Lab-Tek II Chamber Slide, Nalge Nunc International Co.). After an overnight incubation at 37 °C, the medium was removed, **6** (0.2 mL, ~5 μCi) in PBS (0.01 mol/L) was added, and the cells were re-incubated for 24 h. The slides were then washed in 0.01 mol/L PBS (pH 7.4), and the cells were fixed in ice-cold ethanol (−20 °C) for 10 min. After the slides were dried, they were dipped vertically into Kodak NTB-2 emulsion melted at 45 °C, withdrawn, and left to drain and gel. The slides were stored at 4 °C in a black box containing Drierite (anhydrous $CaSO_4$). After exposure (3 days to 1 week), the emulsion-coated slides were dipped at room temperature in Kodak developer D-19 for 5 min, washed in distilled water, immersed in Kodak fixer for 5 min, and rinsed again in distilled water. Finally, the nuclei were stained with DAPI with mount (Vecta Shield) and the slides viewed under a fluorescence (DAPI nuclei)/light (ARG grains) microscope.

Biodistribution of 6 in Normal Mice. To determine normal-tissue localization of **6**, each mouse ($n = 5$/group, total three groups) received an intravenous injection (lateral tail vein) of 5 μCi carrier-free, radioiodinated prodrug in 0.1 mL PBS (0.01 mol/L, pH 7.4). The mice were sacrificed at 24 h, the following organs and tissues were dissected and weighed, and their radioactivity determined in a gamma counter: blood, heart, lungs, liver, spleen, kidneys, fat, bladder, urine, stomach, small intestine, large intestine, muscle, skin, bone, thymus, and thyroid. Based on the injected activity and the weight of these fluids, tissues, and organs, the percentage injected dose per gram (% ID/g) was then calculated.

Supporting Information Available: Lineweaver−Burk plot of PLAP-dependent conversion of prodrug **4** to drug **2**. This material is available free of charge via the Internet at http://pubs.acs.org.

References

(1) Denny, W. A. Tumor-activated prodrugs−a new approach to cancer therapy. *Cancer Invest.* **2004**, *22*, 604−619.

(2) Philpott, G. W.; Shearer, W. T.; Bower, R. J.; Parker, C. W. Selective cytotoxicity of hapten-substituted cells with an antibody-enzyme conjugate. *J. Immunol.* **1973**, *111*, 921−929.

(3) Antoniw, P.; Springer, C. J.; Bagshawe, K. D.; Searle, F.; Melton, R. G.; Rogers, G. T.; Burke, P. J.; Sherwood, R. F. Disposition of the prodrug 4-(bis(2-chloroethyl)amino)benzoyl-L-glutamic acid and its active parent drug in mice. *Br. J. Cancer* **1990**, *62*, 909−914.

(4) Springer, C. J.; Antoniw, P.; Bagshawe, K. D.; Wilman, D. E. V. Comparison of half-lives and cytotoxicity of *N*-chloroethyl-4-amino and *N*-mesyloxyethyl-benzoyl compounds, products of prodrugs in antibody-directed enzyme prodrug therapy (ADEPT). *Anticancer Drug Des.* **1991**, *6*, 467−479.

(5) Bagshawe, K. D. Antibody-directed enzyme prodrug therapy. *Clin. Pharmacokinet.* **1994**, *27*, 368−376.

(6) Senter, P. D.; Schreiber, G. J.; Hirschberg, D. L.; Ashe, S. A.; Hellström, K. E.; Hellström, I. Enhancement of the *in vitro* and *in vivo* antitumor activities of phosphorylated mitomycin C and etoposide derivatives by monoclonal antibody−alkaline phosphatase conjugates. *Cancer Res.* **1989**, *49*, 5789−5792.

(7) Melton, R. G.; Sherwood, R. F. Antibody−enzyme conjugates for cancer therapy. *J. Natl. Cancer Inst.* **1996**, *88*, 153−165.

(8) Cheng, T.-L.; Chen, B.-M.; Chern, J.-W.; Wu, M.-F.; Roffler, S. R. Efficient clearance of poly(ethylene glycol)-modified immunoenzyme with anti-PEG monoclonal antibody for prodrug cancer therapy. *Bioconjugate Chem.* **2000**, *11*, 258−266.

(9) Greco, O.; Dachs, G. U. Gene directed enzyme/prodrug therapy of cancer: historical appraisal and future prospectives. *J. Cell. Physiol.* **2001**, *187*, 22−36.

(10) Breistøl, K.; Hendriks, H. R.; Berger, D. P.; Langdon, S. P.; Fiebig, H. H.; Fodstad, Ø. The antitumour activity of the prodrug *N*-L-leucyl-doxorubicin and its parent compound doxorubicin in human tumour xenografts. *Eur. J. Cancer* **1998**, *34*, 1602−1606.

(11) DeFeo-Jones, D.; Garsky, V. M.; Wong, B. K.; Feng, D.-M.; Bolyar, T.; Haskell, K.; Kiefer, D. M.; Leander, K.; McAvoy, E.; Lumma, P. K.; Wai, J.; Senderak, E. T.; Motzel, S. L.; Keenan, K.; Van Zwieten, M.; Lin, J. H.; Freidinger, R.; Huff, J.; Oliff, A.; Jones, R. E. A peptide−doxorubicin 'prodrug' activated by prostate-specific antigen selectively kills prostate tumor cells positive for prostate-specific antigen *in vivo*. *Nature Med.* **2000**, *6*, 1248−1252.

(12) Wong, B. K.; DeFeo-Jones, D.; Jones, R. E.; Garsky, V. M.; Feng, D.-M.; Oliff, A.; Chiba, M.; Ellis, J. D.; Lin, J. H. PSA-specific and non-PSA-specific conversion of a PSA-targeted peptide conjugate of doxorubicin to its active metabolites. *Drug Metab. Dispos.* **2001**, *29*, 313−318.

(13) Kassis, A. I.; Harapanhalli, R. S. Methods for tumor diagnosis and therapy. U.S. Patent Appl. 09/839,779, 2001.

(14) Ho, N.; Harapanhalli, R. S.; Dahman, B. A.; Chen, K.; Wang, K.; Adelstein, S. J.; Kassis, A. I. Synthesis and biologic evaluation of a radioiodinated quinazolinone derivative for enzyme-mediated insolubilization therapy. *Bioconjugate Chem.* **2002**, *13*, 357−364.

(15) Chen, K.; Wang, K.; Kirichian, A. M.; Al Aowad, A. F.; Iyer, L. K.; Adelstein, S. J.; Kassis, A. I. *In silico* design, synthesis, and biological evaluation of radioiodinated quinazolinone derivatives for alkaline phosphatase−mediated cancer diagnosis and therapy. *Mol. Cancer Ther.* **2006**, *5*, 3001−3013.

(16) Pospisil, P.; Wang, K.; Al Aowad, A. F.; Iyer, L. K.; Adelstein, S. J.; Kassis, A. I. Computational modeling, synthesis, and evaluation of a novel prodrug for targeting the extracellular space of prostate tumors. *Cancer Res.,* in press.

(17) Wang, K.; Adelstein, S. J.; Kassis, A. I. Evaluation of chemical, physical and biologic properties of a potential anti-tumor radioiodinated quinazolinone derivative. *Bioconjugate Chem.,* in press.

(18) Herz, F. Alkaline phosphatase isozymes in cultured human cancer cells. *Experientia* **1985**, *41*, 1357−1361.

(19) Harris, H. The human alkaline phosphatases: what we know and what we don't know. *Clin. Chim. Acta* **1990**, *186*, 133−150.

(20) Byers, D. A.; Fernley, H. N.; Walker, P. G. Studies on alkaline phosphatase: catalytic activity of human-placental alkaline-phosphatase variants. *Eur. J. Biochem.* **1972**, *29*, 205−209.

(21) McComb, R. B.; Bowers, G. N., Jr. Alkaline phosphatase and the International Clinical Enzyme Scale. *Am. J. Clin. Pathol.* **1985**, *84*, 67−73.

(22) Le Du, M. H.; Stigbrand, T.; Taussig, M. J.; Ménez, A.; Stura, E. A. Crystal structure of alkaline phosphatase from human placenta at 1.8 Å resolution: implication for a substrate specificity. *J. Biol. Chem.* **2001**, *276*, 9158−9165.

(23) Suzuki, H.; Iino, S.; Endo, Y.; Torii, M.; Miki, K.; Oda, T. Tumor-specific alkaline phosphatase in hepatoma. *Ann. N. Y. Acad. Sci.* **1975**, *259*, 307−320.

(24) Miyayama, H.; Doellgast, G. J.; Memoli, V.; Gandbhir, L.; Fishman, W. H. Direct immunoperoxidase staining for Regan isoenzyme of alkaline phosphatase in human tumor tissues. *Cancer* **1976**, *38*, 1237−1246.

(25) Benham, F.; Cottell, D. C.; Franks, L. M.; Wilson, P. D. Alkaline phosphatase activity in human bladder tumor cell lines. *J. Histochem. Cytochem.* **1977**, *25*, 266−274.

(26) Benham, F. J.; Povey, M. S.; Harris, H. Placental-like alkaline phosphatase in malignant and benign ovarian tumors. *Clin. Chim. Acta* **1978**, *86*, 201−215.

(27) Benham, F. J.; Harris, H. Human cell lines expressing intestinal alkaline phosphatase. *Proc. Natl. Acad. Sci. U.S.A.* **1979**, *76*, 4016−4019.

(28) Fishman, W. H.; Inglis, N. I.; Stolbach, L. L.; Krant, M. J. A serum alkaline phosphatase isoenzyme of human neoplastic cell origin. *Cancer Res.* **1968**, *28*, 150−154.

(29) Dempo, K.; Elliott, K. A. C.; Desmond, W.; Fishman, W. H. Demonstration of gamma-glutamyl transferase, alkaline phosphatase, CEA and HCG in human lung cancer. *Oncodev. Biol. Med.* **1981**, *2*, 21−37.

(30) Nouwen, E. J.; Pollet, D. E.; Schelstraete, J. B.; Eerdekens, M. W.; Hänsch, C.; Van de Voorde, A.; De Broe, M. E. Human placental alkaline phosphatase in benign and malignant ovarian neoplasia. *Cancer Res.* **1985**, *45*, 892−902.

(31) Nouwen, E. J.; Pollet, D. E.; Eerdekens, M. W.; Hendrix, P. G.; Briers, T. W.; De Broe, M. E. Immunohistochemical localization of placental alkaline phosphatase, carcinoembryonic antigen, and cancer antigen 125 in normal and neoplastic human lung. *Cancer Res.* **1986**, *46*, 866−876.

(32) Wick, M. R.; Swanson, P. E.; Manivel, J. C. Placental-like alkaline phosphatase reactivity in human tumors: an immunohistochemical study of 520 cases. *Hum. Pathol.* **1987**, *18*, 946−954.

(33) Alberts, I. L.; Nadassy, K.; Wodak, S. J. Analysis of zinc binding sites in protein crystal structures. *Protein Sci.* **1998**, *7*, 1700−1716.

(34) Buzko, O. V.; Bishop, A. C.; Shokat, K. M. Modified AutoDock for accurate docking of protein kinase inhibitors. *J. Comput. Aided Mol. Des.* **2002**, *16*, 113−127.

(35) Hu, X.; Shelver, W. H. Docking studies of matrix metalloproteinase inhibitors: zinc parameter optimization to improve the binding free energy prediction. *J. Mol. Graph. Model.* **2003**, *22*, 115−126.

(36) Morris, G. M.; Goodsell, D. S.; Halliday, R. S.; Huey, R.; Hart, W. E.; Belew, R. K.; Olson, A. J. Automated docking using a Lamarckian genetic algorithm and an empirical binding free energy function. *J. Comput. Chem.* **1998**, *19*, 1639−1662.

(37) Tuttle, C. T. T.; Seabrook, S. A.; Wise, L. E.; Katsifis, A.; Knott, R. B.; Yates, B. F. Molecular modelling and design of radiolabelled complexes for melanoma diagnosis. *Aust. J. Chem.* **2004**, *57*, 87−96.

(38) Llinas, P.; Stura, E. A.; Ménez, A.; Kiss, Z.; Stigbrand, T.; Millán, J. L.; Le Du, M. H. Structural studies of human placental alkaline phosphatase in complex with functional ligands. *J. Mol. Biol.* **2005**, *350*, 441−451.

(39) Doellgast, G. J.; Homesley, H. D. Placental-type alkaline phosphatase in ovarian cancer fluids and tissues. *Obstet. Gynecol.* **1984**, *63*, 324−329.

(40) Epenetos, A. A.; Travers, P.; Gatter, K. C.; Oliver, R. D. T.; Mason, D. Y.; Bodmer, W. F. An immunohistological study of testicular germ cell tumours using two different monoclonal antibodies against placental alkaline phosphatase. *Br. J. Cancer* **1984**, *49*, 11−15.

(41) McDicken, I. W.; McLaughlin, P. J.; Tromans, P. M.; Luesley, D. M.; Johnson, P. M. Detection of placental-type alkaline phosphatase in ovarian cancer. *Br. J. Cancer* **1985**, *52*, 59−64.

(42) Pollet, D. E.; Nouwen, E. J.; Schelstraete, J. B.; Renard, J.; Van de Voorde, A.; De Broe, M. E. Enzyme−antigen immunoassay for human placental alkaline phosphatase in serum and tissue extracts, and its application as a tumor marker. *Clin. Chem.* **1985**, *31*, 41−45.

(43) Wang, K.; Adelstein, S. J.; Kassis, A. I. Radiotracer-based method for determining water solubility of highly insoluble compounds. *J. Label. Compd. Radiopharm.* **2006**, *49*, 773−788.

(44) Guex, N.; Peitsch, M. C. SWISS-MODEL and the Swiss-Pdb viewer: an environment for comparative protein modeling. *Electrophoresis* **1997**, *18*, 2714−2723.

(45) Weiner, S. J.; Kollman, P. A.; Case, D. A.; Singh, U. C.; Ghio, C.; Alagona, G.; Profeta, S., Jr.; Weiner, P. A new force field for molecular mechanical simulation of nucleic acids and proteins. *J. Am. Chem. Soc.* **1984**, *106*, 765−784.

(46) Accelrys Software Incorporated. http://www.accelrys.com/products/insight/.

(47) Fujitsu America Incorporated, CAChe 5.0. http://www.cachesoftware.com/cache/index.shtml.

(48) Stote, R. H.; Karplus, M. Zinc binding in proteins and solution: a simple but accurate nonbonded representation. *Proteins* **1995**, *23*, 12−31.

(49) OriginLab Corporation Origin 7.0. http://www.originlab.com/.